Quasicrystal surfaces: structure and potential as templates

2002 J. Phys.: Condens. Matter 14 R119

(http://iopscience.iop.org/0953-8984/14/4/201)

INSTITUTE OF PHYSICS PUBLISHING JOURNAL OF PHYSICS: CONDENSED MATTER

J. Phys.: Condens. Matter **14** (2002) R119–R144 PII: S0953-8984(02)13731-3

TOPICAL REVIEW

Quasicrystal surfaces: structure and potential as templates

Rónán McGrath[1,3], Julian Ledieu[1], Erik J Cox[1] and Renee D Diehl[2]

[1] Surface Science Research Centre, The University of Liverpool, Liverpool L69 3BX, UK
[2] Department of Physics, Pennsylvania State University, University Park, PA 16802, USA

E-mail: mcgrath@liv.ac.uk

Received 23 July 2001, in final form 25 October 2001
Published 18 January 2002
Online at stacks.iop.org/JPhysCM/14/R119

Abstract

We present a review of recent progress in determining the surface structure of quasicrystals, with emphasis on their connections to mathematical tiling models. The review focusses in particular on the five-fold surface of icosahedral Al–Pd–Mn and the ten-fold surface of decagonal Al–Ni–Co. We also assess their potential as templates for the formation of two-dimensional quasicrystalline overlayers with reference to recent investigations of atomic and molecular adsorption.

(Some figures in this article are in colour only in the electronic version)

1. Introduction

In the science of crystallography, symmetry is of paramount importance and has provided the framework for the classification of the possible types of crystal structures—the 230 crystallographic space groups. A crystal (until 1992) was defined as a space lattice plus a basis of atoms associated with each lattice point. One of the defining symmetry properties of a lattice is that of rotational symmetry: a lattice possesses n-fold rotational symmetry if rotation of the lattice through an angle of $2\pi/n$ transforms it into itself. A theorem which is easily proven at undergraduate level tells us that in this framework, $n = 1, 2, 3, 4, 6$ are the only possible values of n for a periodic lattice [1].

The discovery of quasicrystals shook this framework considerably [2]. On April 8th 1982, Dan Shechtman, then of the Weizman Institute in Israel but on sabbatical leave at the then National Bureau of Standards in Washington DC, was imaging some rapidly quenched aluminium–manganese alloys in an electron microscope. Using the instrument in a diffraction mode, he observed some grains of the material which gave sharp peaks with the symmetry of a three-dimensional icosahedron. An icosahedron has six five-fold symmetry axes which,

[3] Author to whom any correspondence should be addressed.

by the theorem stated previously, cannot exist in periodic structures. Shechtman has given an entertaining account of the dramatic story of this discovery and how the results finally came to be accepted by the scientific community [3] (including the rejection of a manuscript by a leading journal). The work initially encountered the opposition of many notable crystallographers, including Linus Pauling, a double Nobel prize winner [4]. Subsequent results verified beyond any doubt the existence of these materials and hundreds of quasicrystalline compounds have been discovered in the intervening years. In 1992 the redefinition of the crystal was undertaken by the International Union of Crystallography [5], motivated by the existence of quasicrystals. A crystal is now 'any solid with an essentially discrete diffraction pattern'. (The resolution of these symmetry properties with the theorem quoted above is because the structure of quasicrystals is non-periodic. This will be discussed further in section 2.) Today the field is burgeoning, with frequent discoveries of new families of quasicrystals, most recently the Cd-based stable binary quasicrystalline alloys [6].

This paper focusses not on bulk quasicrystals but on their surfaces. Why should the surfaces of these materials be of interest? A very fundamental question is whether the surfaces of quasicrystals as prepared using the techniques available to surface science are themselves *quasicrystalline*. This is not a trivial question and much effort has been expended over the past few years in addressing this point. The sputtering and annealing methodology of surface preparation has the disadvantage that lighter elements sputter preferentially, which can lead to a surface composition outside the usually narrow composition range within which the bulk quasicrystalline phase is found. Furthermore, because they are aperiodic materials, the most powerful tools of surface structural determination, i.e. diffraction methods, have only limited applicability as the analysis of results is based on a formalism developed for periodic structures. Much of this review is concerned with the study of the structure of the clean surfaces of quasicrystals using scanning tunnelling microscopy (STM) and the methodology that we and others have developed and employed to analyse the resulting images and compare them with the predictions of well-established theoretical models of the bulk structure. These models make specific predictions about the structural patterns which may be expected when a planar termination of the bulk structure is made. In section 2 we outline these models together with the advances in the theory of tilings and coverings which have been very important to their development. Our experience, detailed later in sections 3 and 4, is that the surfaces can indeed be prepared in a quasicrystalline form which matches well with our expectations based on bulk models.

Once it has been established that high quality quasicrystalline surfaces can be prepared, this opens the door to a myriad of exciting research opportunities. Over the past 40 years, an enormous database of information on surfaces of periodic materials has built up in the scientific literature. There is a wealth of detailed information on such topics as surface relaxation and reconstruction, surface electronic states, the kinetics and dynamics of surface chemical reactions, surface morphology and roughness, growth and interface formation, surface reactivity and so on. There is an intrinsic interest in discovering whether the generally accepted concepts which have been found to apply to crystalline surfaces are also true when the surface is quasicrystalline. There has been progress in some of these areas; for example despite the lack of translational symmetry, delocalized quasicrystalline valence electron states have been found to exist in *d*-AlNiCo [7]. Nevertheless the area of surface studies is largely untapped with considerable scope for development. In section 5 we describe some of our initial studies of adsorption on quasicrystal surfaces.

Another area with much potential for further development lies in the possible applications of quasicrystals. Some of these possible applications directly concern the quasicrystal surface. One example is the use of quasicrystals as catalyst materials: Tsai and Yoshimuro

have demonstrated the use of the AlCuFe quasicrystal as a catalyst for steam-reforming of methanol [8]. Another example is in the area of tribological properties, which have been found to be somewhat unusual. These include good corrosion resistance [9], low coefficients of friction that rival Teflon and good wear-resistance [10], and low surface energies giving non-stick behaviour [11]. These properties make them a potentially attractive alternative to conventional, chemically-based platings for machine parts and other coatings applications. The question of whether these properties are determined by the quasicrystalline structure of the surface can still be considered to be open. An intriguing suggestion is that the lack of commensurability between a quasicrystalline surface and a surface of a periodic material influences the friction properties [12]. However the area of applications is beyond our scope and readers are referred to [13] for a summary and to a recent conference proceedings [14] for the latest developments.

Finally, nanoscience is considered to be of immense importance for 21st Century technology (e.g. [15]). The use of quasicrystalline arrays has already been probed in macroscopic photonic technologies (e.g. [16]). The development of quasicrystalline nanostructures would lead to new technological possibilities; furthermore two-dimensional quasicrystalline arrays of atoms/molecules can be expected to have interesting and unusual properties. The best possibility for the creation of such nanostructures and arrays would appear to be the use of quasicrystalline surfaces as templates for atomic and molecular adsorption; some initial results in this area are discussed in section 5.3.

2. Tilings and coverings

2.1. Historical perspective

In order to provide a framework for the discussion of the experimental results on quasicrystal surfaces we first introduce the topic of tilings and coverings. By a 'tiling' we mean a placement of one or more tiles with no overlaps such that the plane is completely covered; a 'covering' is a placement of tiles such that the plane is completely covered but where overlaps of tiles are allowed. (More rigorous definitions may be found in the book of Grünbaum and Shephard entitled 'Tilings and Patterns' [17].) The symmetry theorem referred to in the second paragraph of the introduction applies also to the case of two dimensions: in particular it is not possible to tile a plane or surface periodically such that the tiling has a five- or ten-fold symmetry.

Nevertheless, there have been many attempts at tiling of the plane where tiles or groups of tiles with elements of five-fold and ten-fold symmetry have been incorporated. The tenth Century Arabic mathematician Mohammad Abu'l-Wafa Al-Buzjani introduced the use of tiles of so-called 'kite' and 'dart' shape which anticipated later 20th Century work. The German artist Albrecht Dürer (1471–1528) became interested in the geometry of the plane through his investigations of perspective in art. In his book '*A Manual of Measurements of Lines, Areas and Solids by Compass and Ruler*', published in 1525, he made use of regular pentagons to produce tilings in which the gaps (or 'frustrations') were filled by rhombuses [18]. Elements of five-fold symmetry have been a feature of Islamic tiling art; for example Makovicky in [19] describes a 15th Century decoration of an Iranian tomb which has such symmetries. Johannes Kepler (1571–1630) was a natural philosopher who encapsulated his world view in his monumental opus 'Harmonices Mundi' (the Harmony of the Worlds) published in 1525 [20]. In this work he outlined his views on the harmonic principles which were thought to underlie architecture, geometry, music, astronomy ('the harmony of the spheres') and other areas of human knowledge. As part of this work he described a tiling shown in figure 1 (labelled '*Aa*') involving pentagons, pentagrams (pentagonal stars), decagons and double decagons which has

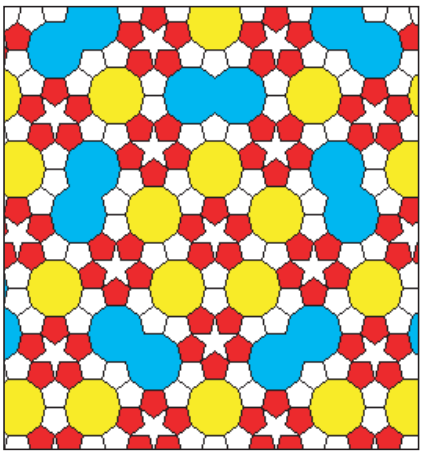

Figure 1. Kepler '*Aa*' tiling.

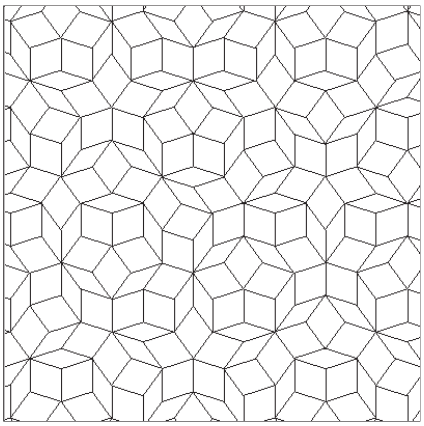

Figure 2. Penrose tiling generated using the program 'Quasitiler' [24].

strong elements of five- and ten-fold symmetry. This tiling, (although known to be periodic) has been much commented on (see e.g. [21]).

The mathematical basis of tilings has been described by Grünbaum and Shephard [17], and in one chapter they outline some of the many 20th Century advances in the area of aperiodic tilings (tilings which do not have a repeating pattern or unit cell). This area had a major impact on popular scientific culture with the discovery announced by Roger Penrose in his paper 'The rôle of aesthetics in pure and applied mathematical research' [22] of a set of prototiles which when assembled according to strict edge matching rules produced a tiling of the plane which had strong elements of five- and ten-fold symmetry and was forcibly aperiodic. Figure 2 shows an example of such a Penrose tiling. Penrose himself has described the background to this discovery elsewhere [23]. The fact that Penrose tilings had local elements of five- and ten-fold symmetry but were aperiodic seemed to provide an excellent basis for their exploration as possible models for the structures of the newly-discovered quasicrystals in the early 1980s.

Three-dimensional aperiodic tilings can be generated by the cut and projection method from a periodic lattice in a higher-dimensional space. This method is described in detail

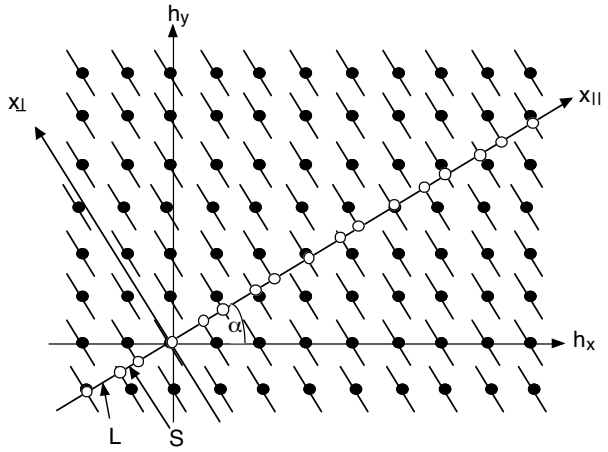

Figure 3. Construction of a one-dimensional quasicrystal via a two-dimensional hyperlattice (cut-method). The 'tiles' are the resulting long (L) and short (S) line segments; after [27].

in [25–27]. Figure 3 shows the construction of a one-dimensional quasicrystal. A two-dimensional hyperlattice (h_x, h_y) is defined. A second coordinate system $(x_\parallel, x_\perp)$, representing physical space and orthogonal space, respectively, is rotated by an angle α. α is chosen to be the inverse tangent of the 'golden mean', $\tau = 1/2 * (1 + \sqrt{5}) = 1.618\,03\ldots$. The hyperlattice points are decorated by objects which are extended along the orthogonal space $x_\perp$. The atomic positions in real space are located where these objects cut $x_\parallel$. The resulting one-dimensional quasicrystal is aperiodic but perfectly ordered. It can also be represented by two unit cells (with long (L) and short (S) lattice parameters, the ratio of which equals τ). These are arranged according to strict matching rules. Such a construction has close similarities with the Fibonacci sequence [28][4], where the value of successive terms f_n are related by:

$$\lim_{n\to\infty} \frac{f_{n+1}}{f_n} = \tau. \tag{1}$$

2.2. Icosahedral tiling models

The projection method has been applied very successfully to modelling icosahedral quasicrystals. This approach was pioneered by Katz, Gratias and Elser [29, 30] and has since been explored in detail by Kramer, Papadopolos and Kasner [31–33]. Here the cut and projection is applied to a six-dimensional face-centred hypercubic lattice (labelled D_6). This leads to a three-dimensional quasicrystalline tiling $\mathcal{T}^{*(2F)}$. This tiling is decorated by Bergman (and automatically Mackay) polytopes to give the atomic positions [31]. These polytopes (shown in figure 4) are clusters of atoms arranged in a specific geometry to give the correct bulk stoichiometry.

All of the vertices of the $\mathcal{T}^{*(2F)}$ tiling can be embedded in a sequence of planes orthogonal to a five-fold symmetry axis of an icosahedron [32]. The edge length of the tiling is matched to an experimentally derived value in order to introduce a physical scale into the model.

[4] The Fibonacci sequence consists of terms such that the nth term is the sum of the $(n-1)$ and $(n-2)$ terms; furthermore the ratio of successive terms approaches the golden ratio τ as n becomes large; τ is an irrational number whose first few terms are $\tau = 1.618\ldots$.

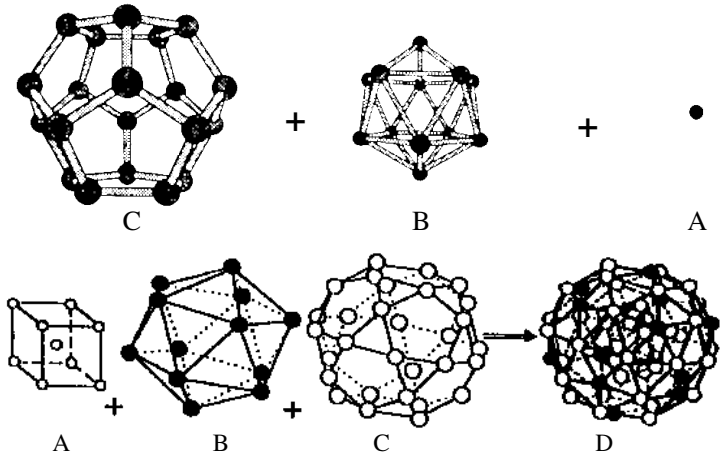

Figure 4. Top: representation of a Bergman cluster (33 atoms). The cluster is defined by a central atom A, a middle shell B (icosahedron: 12 atoms) and an outer shell C (dodecahedron: 20 atoms), from [34]. Bottom: representation of a pseudo-Mackay icosahedron D (51 atoms). The cluster is defined by an inner shell A (partially occupied dodecahedron: nine atoms), middle shell B (icosahedron: 12 atoms) and an outer shell (icosidodecahedron: 30 atoms), from [33].

2.3. Decagonal tiling models

The results of quantitative structure determinations of decagonal quasicrystals indicate that the three-dimensional structure consists of quasiperiodic atomic layers which are stacked according to different sequences. An equivalent structural description can be formulated in terms of columnar clusters parallel to the ten-fold axis [35]. One way of describing this columnar cluster model is as a three-dimensional extension of a two-dimensional Penrose tiling. In the Penrose tiling picture, the atoms are arranged into clusters which are analogous to the rhombic Penrose tiles. The interactions connecting clusters can be compared to the Penrose matching rules for tiles.

However, recently Steinhardt *et al* [36] have proposed a different model for the quasicrystalline structure of $Al_{72}Ni_{20}Co_8$; a single repeating 'quasi-unit-cell', which is illustrated in figure 5. This picture utilizes identical clusters as repeating units. Unlike a periodic unit cell, however, these clusters can share atoms, i.e. they can overlap. Many theoretical overlapping cluster models have since emerged with overlap rules constraining the merging of neighbouring clusters. These models do not force a unique structure—for example Burkov's model can be compared to a binary tiling with an infinite number of possible atomic arrangements [37].

Gummelt has shown that atomic clusters and overlap rules can be chosen so as to force a unique atomic arrangement which is isomorphic to a Penrose tiling [39]. Previously, the widely accepted view was that two types of cluster were necessary to force quasiperiodicity but Gummelt showed that instead of the two incommensurate lengths arising from two different tile shapes, they can also arise from the overlap rules which allows only two nearest-neighbour distances between clusters. In two dimensions the clusters are replaced by decagonal tiles which overlap covering the two-dimensional plane. Gummelt showed that with the correct overlap rules, these decagonal tiles can force a perfect quasiperiodic tiling. Therefore, to determine the atomic structure one must only determine the atomic distribution within the decagonal tile. Steinhardt *et al* have proposed a model for the atomic structure for decagonal $Al_{72}Ni_{20}Co_8$ shown in figure 6.

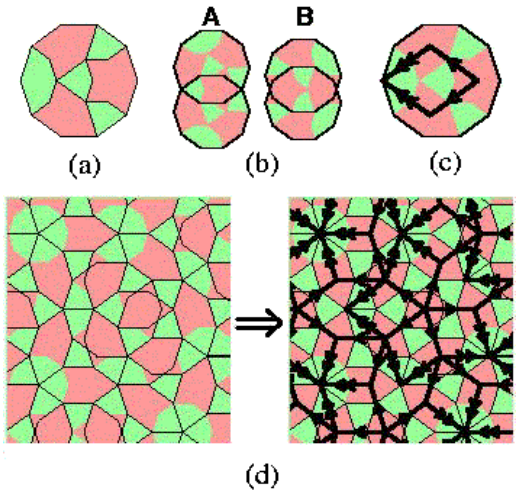

Figure 5. A quasiperiodic tiling can be forced using marked decagons as shown in (*a*). Decagons may only overlap if the shaded regions overlap. This leads to two possibilities where the overlapped area is either small (A-type) or large (B-type) as shown in (*b*). If each decagon is inscribed with an obtuse rhombus as in (*c*), a tiling of overlapping decagons (*d*, left) is converted into a Penrose tiling (*d*, right); from [38].

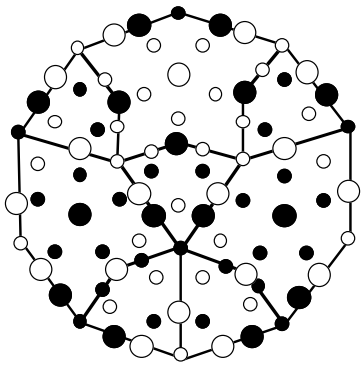

Figure 6. A candidate model for the atomic decoration of the decagonal quasi-unit-cell. Large circles represent Ni and Co; small circles Al. The structure has two distinct layers along the periodic *c*-axis. Solid circles represent $c = 0$, open circles $c = 1/2$; after [40].

The resulting structure is consistent with results from electron microscopy [41–44] (see figure 7) and x-ray diffraction, providing a better fit than previous models, including Penrose tiling [36].

The quasi-unit-cell and Penrose tile pictures are real-space descriptions of quasicrystals where the structure can be defined by an identical decoration of each quasi-unit-cell or Penrose tile. In the hyperspace model, quasicrystals are viewed as projections from a higher-dimensional periodic, hypercubic lattice. The decoration of this lattice consists of atomic surfaces in this higher-dimensional space (usually five- or six-dimensions). These surfaces project into point atoms in three-dimensions. Thus the quasi-unit-cell picture is a simpler concept since it is much easier to consider atomic arrangements within a single quasi-unit-cell in real three-dimensional space than by decoration of two or more tiles, or by imagining five- or six-dimensional surfaces.

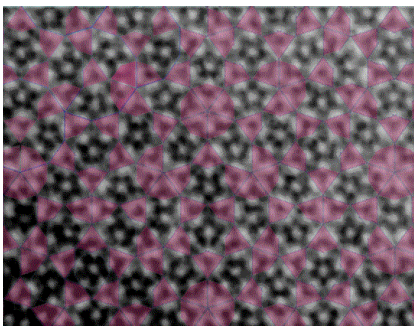

Figure 7. Superposition of a perfect decagon tiling placed over the HAADF image of Al–Ni–Co; from [36].

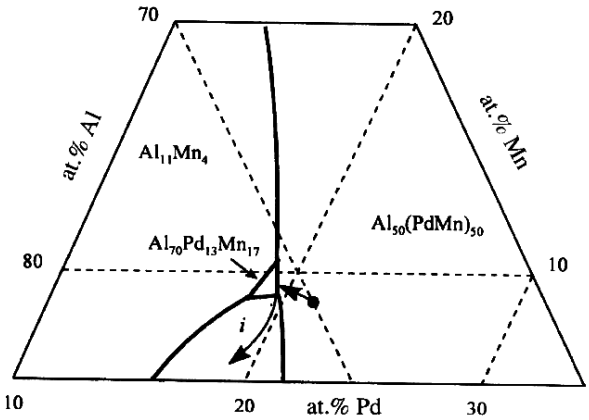

Figure 8. Phase diagram of the Al–Pd–Mn alloy after [48].

3. Structural studies of the five-fold surface of *i*-$Al_{70}Pd_{21}Mn_9$

3.1. The cleaved surface

Due to the narrow icosahedral region of the phase diagram (see figure 8), the surface composition of $Al_{70}Pd_{21}Mn_9$ is critical to producing a surface which has quasicrystalline order. One way of studying the surface without altering the chemical composition from the bulk composition consists of cleaving the sample *in situ* in ultra high vacuum (UHV). Surfaces prepared using this technique have been studied by Ebert *et al* [45–47] using STM. In these studies, a sample grown by the Czochralski method was cleaved along its five-fold symmetry axis under UHV conditions. The surface was then observed to be mirror-like, and the STM images revealed a cluster-like structure. The smallest features observed in these STM images had diameters of between 6 and 10 Å [45, 46]. These were interpreted as being consistent with pseudo-Mackay icosahedral clusters.

The structure and composition of the cleaved surface vary with annealing temperature [45–47]. These changes have been explained by temperature-dependent kinetic effects. Starting at about 370 K, the Mn concentration decreases due to thermal desorption. At around 620 K, the Al concentration decreases as the Pd concentration increases, due to the desorption of Al. Above this temperature, the Mn concentration decreases further due to its desorption from

holes which open up during the heating process. At about 670 K, the Mn concentration increases due to its diffusion from the bulk, and at 820 K, the Al concentration increases and the Pd concentration decreases. These last changes are probably due to Al diffusion and/or Pd evaporation. Finally, above 860 K, a crystalline cubic Al–Pd alloy is formed, with only a small amount of Mn incorporated. The visual appearance of the surface is shiny and metallic after cleaving, followed by a matt appearance after annealing to the intermediate temperatures, and finally shiny and metallic again after the cubic phase is formed.

At the lower annealing temperatures, these surface structures and compositions are quite different from those observed on surfaces which have been sputtered and annealed, due to the selective sputtering of the three elements. At higher temperatures, however, the compositions of the two types of surfaces approach each other and finally coincide. Both types of surfaces form the cubic structure at the highest annealing temperatures. The next section describes surfaces which have been prepared in UHV by sputtering and annealing.

3.2. The sputtered surface

3.2.1. Cleaning procedure. The typical i-$Al_{70}Pd_{21}Mn_9$ sample used in the surface science experiments described here consists of a slab ($10 \times 10 \times 2$ mm^3) cut perpendicular to its five-fold symmetrical axis under atmospheric pressure. Before being inserted in the UHV chamber, the surface of the sample must be polished. Our experience has shown that using 6, 1 and 1/4 μm diamond paste on Kemet cloth (PSU-M type for the 6 μm and the NMH type for the two other pastes) for 1 h gives the best surface preparation in terms of both its visual appearance and its perfection as measured using STM [49]. In most of the experiments described in the following sections, cleaning the surface in UHV consisted of sputtering the surface with 0.5 keV Ar ions, with the sputter angle set at 30° relative to the surface plane.

Detailed studies by the Ames group have shown that the sputtering gas can play a crucial role in exactly how the composition is altered by sputtering [50]. When sputtering, aluminium is removed preferentially, being the lightest element in this alloy. Eventually, a steady-state surface composition is attained which is different from the bulk composition. Minimizing the amount of material sputtered is obviously advantageous for maintaining the surface stoichiometry. The sputtering time needed to reach the steady-state composition is about 5 min for Ne, 4 min for Ar, Kr and Xe, but around 80 min for He. Hence He is the best choice of sputtering gas for minimizing stoichiometric changes [50].

3.2.2. Surface order as a function of temperature. The degree of order in the surface structure can be determined by means of the spot-profile-analysis low-energy electron diffraction (SPALEED) technique [51]. In this section the surface order as a function of temperature as deduced from SPALEED patterns is described. In these experiments, the freshly polished sample was annealed to six different successively-higher temperatures for 90 min each. SPALEED and Auger electron spectroscopy (AES) scans were recorded after cooling the sample following each anneal. The surface was resputtered for 90 min with Ar between each anneal in order to restore the same starting composition.

Figure 9 presents the evolution of the half width at half maximum (HWHM) of the diffraction peak (32002) for annealing temperatures from 740 and 970 K (the indexing of the spots is described in Schaub *et al* [52]). Figure 10 corresponds to the integrated intensity of the peaks (00000) and (32002) for each temperature. From figures 9 and 10 it can be seen that the diffraction peak (32002) sharpens and becomes more intense as the annealing temperature gets higher. The same characteristic is observed for other peaks in the LEED pattern. This is typical of the annealing behaviour for crystalline samples and indicates that the surface becomes more ordered as the annealing temperature is increased.

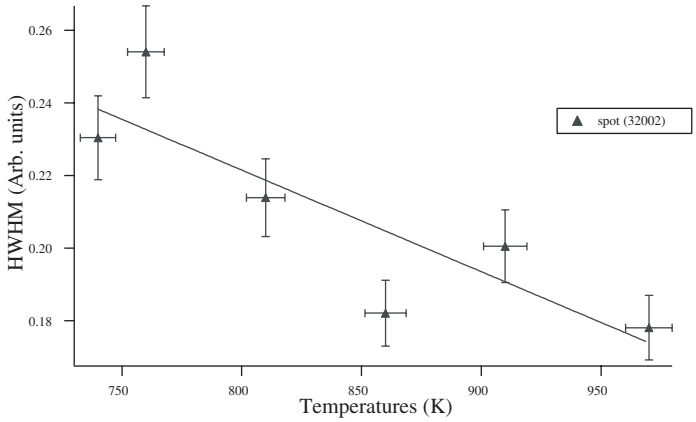

Figure 9. Variation of the HWHM of the diffraction peak (32002) for different annealing temperatures.

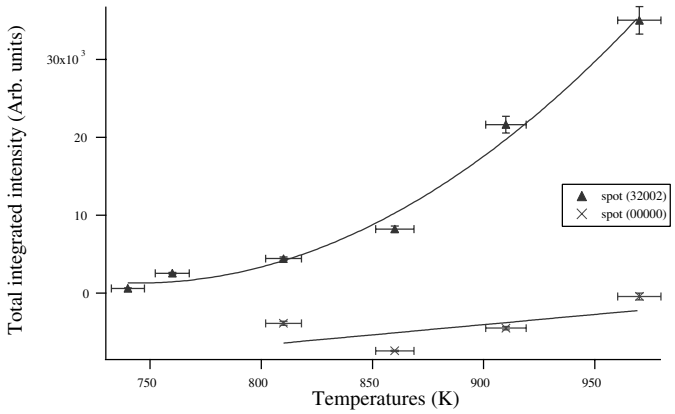

Figure 10. Total integrated intensity of peaks (00000) and (32002) versus temperature.

3.2.3. Metastable crystalline phases. Several metastable structures can be formed by sputtering and annealing to temperatures lower than about 700 K. After sputtering the surface at room temperature with 1.5 keV (Ar^+ ions), x-ray photoelectron spectroscopy (XPS) measurements indicate a surface composition equal to $Al_{50}Pd_{50}$ [53]. The secondary electron imaging (SEI) pattern from this surface can be interpreted as a bcc structure with the [110] direction oriented normal to the surface [53]. Due to the chemical composition of the surface (with depletion of Al and Mn), this structure is thought to be the *B2* CsCl structure. This structure does not extend to the bulk, however, because reflection Laue x-ray diffraction indicates that the icosahedral structure is still intact beneath the surface. If the sample temperature is held between 500 and 700 K while sputtering, a thick (2 nm) decagonal epilayer can be observed by SEI having a composition equal to $Al_{22}Pd_{56}Mn_{22}$ [54].

Using LEED, Shen *et al* found the same crystalline β-Al–Pd phase with the CsCl structure at the surface of the icosahedral sample after sputtering with 1 keV argon ions and annealing the sample to below 700 K [55]. The structural relationship between this phase and the quasicrystalline phase was explained in terms of cubic close packed (ccp) clusters and icosahedral packed (ip) clusters [55, 56]. A LEED pattern from this cubic phase also could be

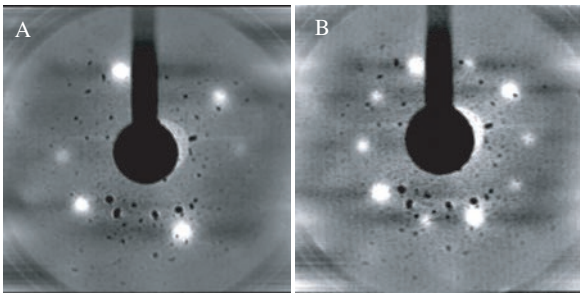

Figure 11. (*a*) LEED pattern recorded at 57 eV from the cubic phase present on the sample after argon sputtering at 500 eV for 30 min. (*b*) LEED pattern recorded at 57 eV after annealing the sample for 10 min to 770 K and then sputtering it for 15 min at 500 eV; from [58].

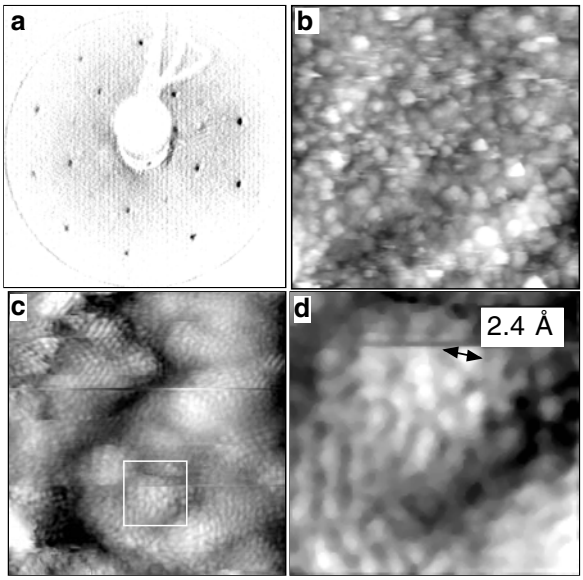

Figure 12. (*a*) LEED pattern (inverted for clarity) obtained after annealing to 800 K at 78.9 eV. (*b*) 400 Å × 400 Å STM image showing a typical clustered surface. (*c*) 100 Å × 100 Å-sized high resolution STM image corresponding to the clustered phase (bias voltage −1.07 V, tip current 1.07 nA). (*d*) 25 Å × 25 Å region of the STM image shown on (*c*); after [62].

observed after sputtering the sample with 500 eV Ar ions for 30 min at room temperature [57]. The cubic (110) structure is evident in figure 11(*a*).

Figure 11(*b*) exhibits the five domains of cubic (110) rotated in respect to each other by 72°. A similar phenomenon is found for Al–Cu–Fe [59] and Al–Ni–Co [60] samples.

3.2.4. Clustered phase. A typical five-fold symmetric LEED pattern obtained after annealing the sample to 800 K for 150 min is shown in figure 12(*a*) [57]. The distances of the outer spots from the centre are related by powers of τ as demonstrated by Guyot and co-workers [61].

STM images from this surface indicate that the surface is rough, with cluster-like protrusions (figures 12(*b*), (*c*)). Features with diameters of 20–30 Å were observed. Higher-resolution scans show substructures having diameters of 2–3 Å (figure 12(*d*)) [57]. An

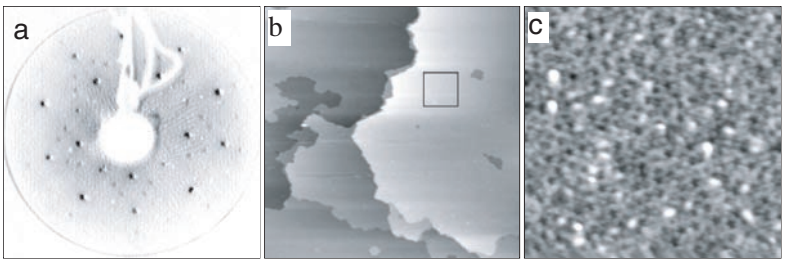

Figure 13. (*a*) LEED pattern recorded after annealing to 970 K at 89.7 eV. (*b*) 1500 Å × 1500 Å image of the surface; the box indicates the size of the image shown in (*c*); (*c*) 200 Å × 200 Å high resolution STM image of a flat terrace (bias voltage 2.29 V, tip current 0.59 nA); after [58].

AES analysis of this surface indicates that the average stoichiometry of the surface is $Al_{72\pm2}Pd_{24\pm2}Mn_{4\pm1}$, which is Mn deficient relative to the bulk composition. The cluster structures look identical to those obtained by Ebert *et al* [46], for surfaces obtained by cleaving and subsequent annealing to 800 K. Shen *et al* [59] have also observed clusters after sputtering and annealing between 700 and 900 K. In that case, the surface composition was estimated to be $Al_{70.5\pm0.8}Pd_{23.1\pm0.6}Mn_{6.4\pm1.2}$ measured by XPS and $Al_{67\pm2}Pd_{26\pm2}Mn_{7\pm1}$ measured by AES. These measurements are consistent with the surface being somewhat Pd enriched and Mn deficient with respect to the initial bulk composition, which is consistent with the evaporative loss of Al and Mn [63].

3.2.5. Terraced phase. This phase is perhaps the most interesting phase of the Al–Pd–Mn quasicrystal from a surface science viewpoint. It can be produced by annealing the surface to about 970 K. The LEED pattern obtained [57, 62] from such a preparation has sharp spots exhibiting five-fold rotational symmetry and a low background intensity (figure 13(*a*)). By analysing the width of the diffraction spots, one can estimate the average terrace width to be about 900 Å [55, 59].

The first STM study done on this surface was by Schaub *et al* [52, 64–66]. After annealing the surface to 1050 K, the STM images indicated a surface composed of flat terraces, separated by steps of two different heights, 4.2 ± 0.3 and 6.8 ± 0.2 Å. The ratio of these two heights is very close to τ. In addition, the sequence of the steps across the area scanned was found to follow a part of the Fibonacci sequence

$$L\underline{HHLHHLHLHH}LHLH\ldots \tag{2}$$

where the underlined part corresponds to the sequence observed by Schaub *et al* [64, 65].

A higher magnification of such terraces reveals five-fold symmetric objects such as five-fold stars and pentagonal depressions (see figure 13(*c*)). These depressions are all orientated in the same way and have the same size. By connecting the edges of these depressions, five sets of parallel lines can be drawn on the STM images. Within these sets of lines, only two separations are observed, of 11.8 ± 0.4 and 7.4 ± 0.4 Å. The ratio of these is equal to the golden mean τ.

The fast Fourier transform (FFT) of figure 13(*c*) (not shown) exhibits ten-fold symmetry. As the FFT process involves an inversion axis this is consistent with five-fold symmetry of the surface. A two-dimensional autocorrelation function calculated for the flat surface (not shown) exhibits a relatively strong spatial correlation over the entire STM image. Schaub and co-workers have compared the experimental autocorrelation function with an autocorrelation function calculated for an Ammann-type pentagrid. The two autocorrelation functions are

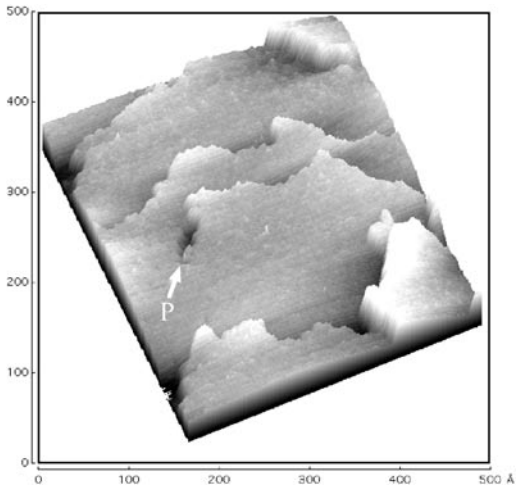

Figure 14. Three-dimensional plot (500 × 500 Å) of a flat terrace showing a screw dislocation. The adjoining step height is estimated at 2.3 ± 0.2 Å, consistent with other work [59]. This step height is observed relatively rarely on this surface.

similar both qualitatively and quantitatively. From this, they inferred that the Ammann grid reproduces the orientations, distribution and spatial correlations of the depressions present on STM images [64, 65].

While the most common defects observed in this phase are surface steps, screw dislocations have also been observed. Figure 14 shows an example of one. One step edge appears to vanish in the middle of the flat terrace at a point labelled 'P'. This is consistent with a screw dislocation as observed in the case of periodic crystals, and its presence supports the idea of describing the surface and bulk structure by atomically dense planes [67–69].

Other groups have carried out STM studies on the same surface. Shen *et al* [59] have obtained similar flat terraces after annealing the sample to 900 K. An additional step height of 2.4±0.2 Å was observed in this study. This step height happens to be the difference between the two previous step heights reported by Schaub *et al* [64, 65]. The STM images recorded in this case do not exhibit the pentagonal depressions shown above, which may relate to a difference in scanning parameters/tip preparation. Shen *et al* [59] have calculated autocorrelation functions from their STM images, from the atomic model proposed by Boudard and co-workers [69] and from a distribution of tangent pseudo-Mackay icosahedra (PMI). By careful examinations of maxima derived from each of the three histograms, they concluded that both PMI and Bergman clusters are consistent with their experimental data and appear as candidates for the origin of the atomic clusters.

A dynamical low-energy electron diffraction analysis (LEED I–V) has also been performed on the flat-terrace phase in order to determine a possible surface structure model [67, 68, 70]. The LEED data were taken after sputtering and annealing the surface to 870–1100 K several times. At this stage the LEED pattern was five-fold symmetric with sharp and intense spots [70]. Gierer *et al* started the LEED analysis by generating a set of possible ideal bulk-like surface terminations, using the bulk model deduced from the x-ray and neutron diffraction analyses by Boudard and co-workers [69]. The model surfaces thus consist of atomically dense layers (parallel to the surface) with different compositions and densities.

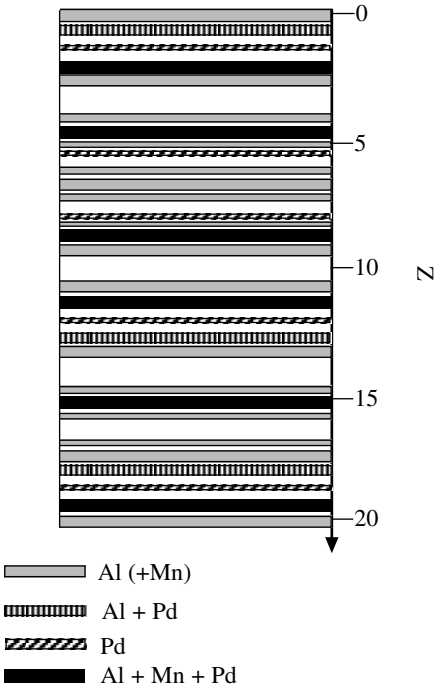

Figure 15. Favoured terminations of the $Al_{70}Pd_{21}Mn_9$ from [70]. The different layers with thickness proportional to the atomic density are drawn at their respective depths Z in Å.

The model layer structure which produced the best fit between the experimental LEED data and the calculated spectra is shown in figure 15. In this figure, the thickness of the lines are proportional to the atomic density in each layer, and each layer has a specific composition. This result indicates that the interlayer spacing between the two topmost layers is 0.38 ± 0.13 Å (a 0.1 Å contraction compared to the bulk value of 0.48 Å [67]). The chemical composition for the first layer is 93% Al and 7% Mn while the second layer is estimated to have 49% Al, 42% Pd and 9% Mn [67, 70]. The overall composition for the two topmost layers is therefore $Al_{77}Pd_{15}Mn_8$ with a two-dimensional density calculated around 0.136 atoms $Å^{-2}$.

Looking at the interlayer spacings of the deeper layers, many can be correlated with the step heights (4.08 and 6.60 Å) obtained by the earlier STM studies [52,64–66]. It was also noted that once orientated along a five-fold axis, each plane of a Mackay cluster has its counterpart in this surface structure determined by the dynamical LEED calculation. Therefore one expects intact PMI to exist in the surface region, with additional atoms filling the spaces between the PMI atoms. This is consistent with the cleaved surface studies of Ebert *et al* [45–47]. In this surface structure model, the features which seem to correspond best to the pentagonal depressions observed using STM [64] are either Mn atoms in the topmost layer surrounded by five atoms of Al or Pd in the second layer, or simply five-fold symmetric vacancies in this surface structure [67, 68, 70].

The STM images from $Al_{70}Pd_{21}Mn_9$ have also been analysed geometrically in order to understand which clusters and tiling rules are the most appropriate to describe the surface [32, 33]. One geometric model is defined as an alternating decoration with Bergman and Mackay polytopes of the vertices of a primitive tiling denoted as $\mathcal{T}^{*(2F)}$. This geometric model is best understood as being composed of 'geared' layers of Bergman polytopes [32]. In

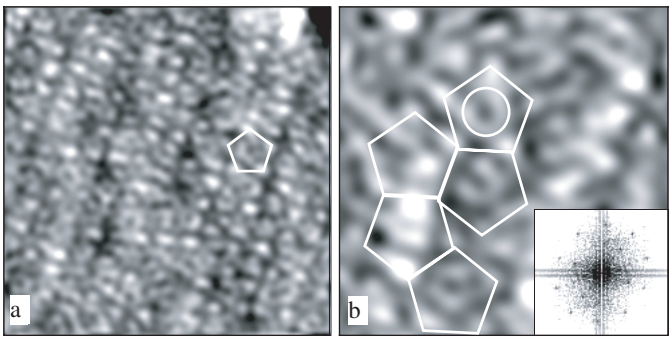

Figure 16. (*a*) 100 Å × 100 Å high resolution STM image obtained on the five-fold surface of the Al–Pd–Mn quasicrystal ($V = 1$ V, $I = 0.3$ nA). (*b*) 50 Å × 50 Å high resolution STM image ($V = 1$ V, $I = 0.3$ nA). A pentagon has been outlined. Inset: the calculated FFT exhibits ten-fold symmetry; after [49].

order to provide the required correspondence with the step heights measured by STM [64], the Bergman clusters proposed in this model have to be cut (producing the 'geared layers'). This model then reproduces the Fibonacci sequences observed by STM in both the step heights and the distribution of pentagonal depressions.

A recent detailed analysis of high-resolution STM images supports the correspondence of the observed terrace structure and this proposed tiling model [49]. High-resolution STM images such as that shown in figure 16(*a*) were obtained using the surface preparation described previously. The visual appearance of the surface at this point was still shiny and metallic. The image in figure 16(*a*) shows atom-sized features as well as larger features (4–6 Å wide) which probably correspond to clusters of a few atoms. The density of pentagonal depressions appears to be approximately three times lower than in figure 13(*b*). A 50 Å × 50 Å STM image from the same surface is shown in figure 16(*b*). Several pentagons having edge lengths equal to 8.0±0.3 Å are outlined on this image. These pentagons are generated by connecting protrusions on the image. In the inset present on figure 16(*b*), a FFT has been calculated for the STM image present on figure 16(*a*) and exhibits ten-fold symmetry.

If the identification of pentagons drawn by connecting STM protrusions as shown in figure 16(*b*) is extended over a larger area, the result produces a tiling as shown in figure 17(*a*). In this tiling, several different shapes, namely rhombuses, boat-like shapes and large five-fold stars are distinguishable.

Figure 17(*b*) represents the theoretical tiling $\mathcal{T}^{*((P1)r)}$ derived from the primitive tiling model $\mathcal{T}^{*(2F)}$, mentioned earlier, which defines the quasiperiodic structure. $\mathcal{T}^{*((P1)r)}$ is denoted as a random Penrose tiling because of the rules of its derivation. $\mathcal{T}^{*((P1)r)}$ clearly matches the geometry of the experimentally derived one (see figure 17(*a*)). The experimental tiling can also be superimposed on one of the dense atomic planes perpendicular to the five-fold axes of the $Al_{70}Pd_{21}Mn_9$ quasicrystal described by Boudard's bulk model [69]. We therefore believe that these STM results correspond to a bulk-terminated surface. The tiling model applied here also predicts large variations of the densities of pentagonal depressions in successive terraces on the surface; however, this prediction has not yet been confirmed by experimental measurements.

3.2.6. Coexistence of two phases. If the sample was annealed to 970 K for a period less than 2 h, a coexistence of the clustered phase and the terraced phase was observed in STM images. The diameters of the clusters obtained were measured to be between 20 and 60 Å, similar to

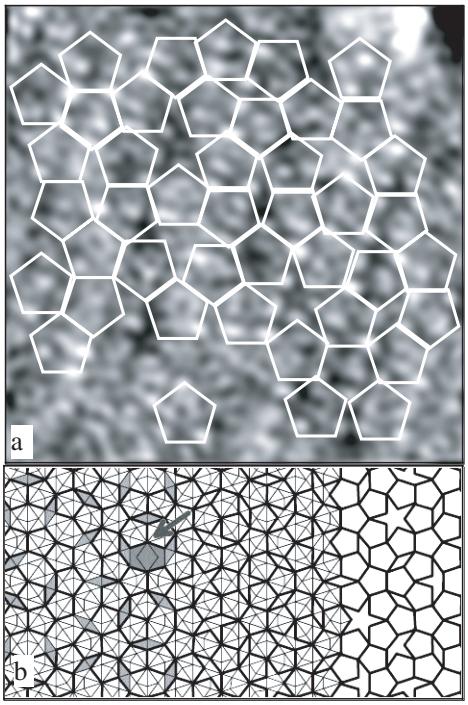

Figure 17. (*a*) Experimental tiling using pentagons on the STM image shown on figure 16(*a*). (A slight distortion (due to the piezoelectric drift) on the STM image has introduced a small mismatch in the tiling.) (*b*) Left side: the tiling $\mathcal{T}^*$ of the plane by the acute rhombus, pentagon and hexagon, locally derived from $\mathcal{T}^{*(A_4)}$. Centre: the construction of the tiling $\mathcal{T}^{*((P1)r)}$. Right side: the tiling $\mathcal{T}^{*((P1)r)}$ without the content of the golden triangles [49].

our previous measurements of the clustered phase described earlier [57]. The different regions labelled on figure 18(*a*) appear to represent three stages in the cluster-to-terrace transition. Note that clusters are shown in contact with the terraced phase. Additionally, clusters (diameters between 20 and 30 Å) in region 2 appear to align in a preferential direction. This feature is shown more clearly on figure 18(*b*). The alignment follows the direction pointed out by the white line.

3.3. Decomposition of the five-fold surface at elevated temperature

If the sample (sputtered or cleaved) is annealed to higher than 970 K (20–30 K higher) for several minutes, a new phase is obtained at its surface [71]. The quasicrystalline structure decomposes into a crystalline phase with its elementary dimensions matching those of orthorhombic Al_3Mn [72]. This dramatic change in surface topography arises from a change in the surface composition. Quantitative fluorescence measurements have been carried out in a scanning electron microscope (SEM) and show a composition of $Al_{75}Pd_6Mn_{19}$ [71]. This is close to Al_3Mn if we accept that Pd may substitute for Mn, or that there may be excess Pd in regions of the surface where the phase transformation is not complete. This decomposition takes place only at a near-surface region (not the entire bulk of the sample) as the terraced phase can be obtained again after mechanical polishing of the sample.

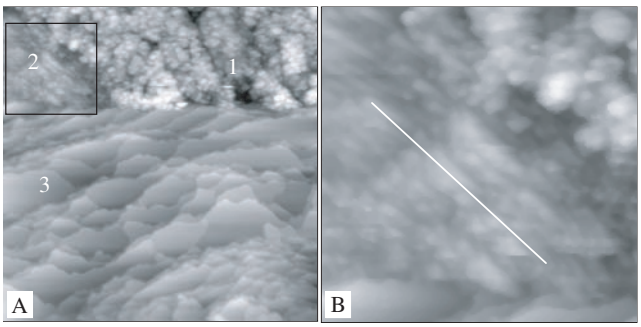

Figure 18. (*a*) 2000 × 2000 Å STM image showing the coexistence of the clustered and terraced phases (bias voltage 1.0 V, tip current 1.0 nA). A line by line quadratic compensation is applied to the image. (*b*) 600 × 600 Å STM image of the framed area in (*a*) showing some preferential alignment of clusters/cluster fragments in region 2 (bias voltage 1.0 V, tip current 1.0 nA); after [62].

3.4. Summary

Despite the differences due to somewhat different stoichiometries, the structures of the cleaved and annealed *i*-$Al_{70}Pd_{21}Mn_9$ quasicrystal surfaces show strong similarities to those which are sputtered and annealed.

Simply sputtering the surface of the sample at room temperature, with or without annealing it to temperatures lower than about 700 K, will produce two crystalline phases (cubic and decagonal [53, 54, 73]). Annealing the sputtered surface to between 700 and 900 K produces a rough topography called the 'clustered phase'. This phase is obtained over a large range of temperatures and for annealing times ranging from 15 min to several hours. At this stage the surface composition is very close to the bulk one [55, 74]. The elementary building block of the clustered phase has not yet been determined nor has the structure. However, when annealed to between 925 and 970 K for 30 min the surface has been found to be consistent with PMI clusters [75].

Annealing the sputtered surface between 900 and 1050 K produces another phase called the 'flat terraced phase'. Its topography is characterized by flat terraces, separated by steps of different heights [59, 64]. Its composition is Pd rich and Mn deficient with respect to the nominal bulk stoichiometry. The first STM images obtained from the surface of the Al–Pd–Mn quasicrystal were analysed by means of a Fibonacci pentagrid [52, 64–66]. Pentagonal depressions are a characteristic of these surfaces. A theoretical model was proposed which consists of 'geared' layers of Bergman clusters [32,33]. Optimization of the surface preparation (see section 3.2.1) allowed atomically-resolved STM images to be obtained. The structures in these images were found to match the tiling $\mathcal{T}^{*((P1)r)}$, which was theoretically derived from $\mathcal{T}^{*(2F)}$. This surface was interpreted as a bulk termination, consistent with LEED studies of the same surface [67, 68].

Finally, the first steps of decomposition of the quasicrystalline phase to a crystalline phase were also observed. A model for this crystalline structure was proposed, in which the length and width of the unit cell are similar to those of orthorhombic Al_3Mn.

4. Structural studies of the ten-fold surface of *d*-$Al_{72}Ni_{11}Co_{17}$

4.1. Surface preparation

Most of the Al–Ni–Co samples used in surface studies are grown using the melt decantation method. After being cut into a wafer which has its major faces perpendicular to the ten-fold

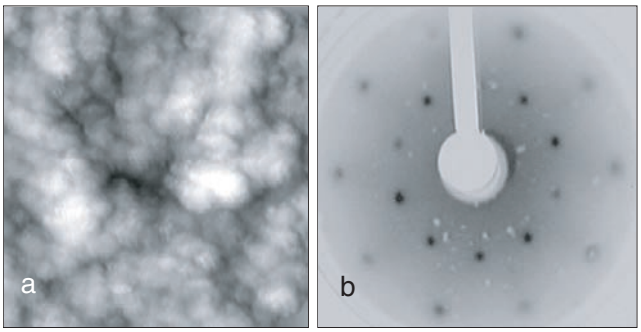

Figure 19. (*a*) STM image of the surface obtained directly after sputtering. (*b*) LEED pattern obtained from this surface showing cubic CsCl pseudo ten-fold pattern; after [77].

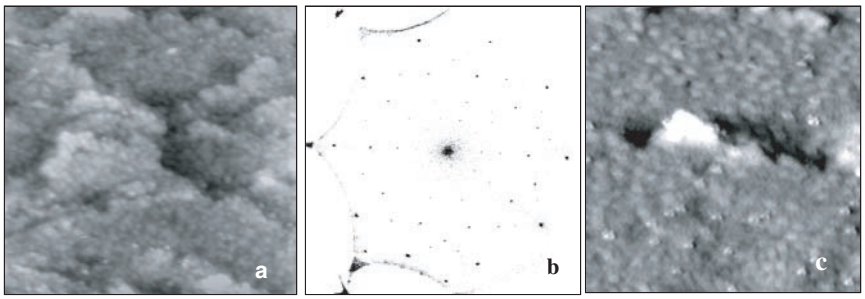

Figure 20. (*a*) 500 × 500 Å STM image obtained after annealing to 725 K for 90 min. (*b*) LEED pattern after annealing to 875 K for 90 min (58 eV)(sample cooled to 100 K). (*c*) 500 × 500 Å STM image after annealing to 875 K for 90 min, showing the three-fold protrusions (−2 V, 1.5 nA) after [77].

axis, the surface is polished. A typical polishing procedure involves successive polishes using 6, 1, and $1/4$ μm diamond paste on Kemet cloth. The in-vacuum preparation typically consists of cycles of Ar ion bombardment (0.5 keV) followed by annealing for 1–2 h. Aluminium, being the lightest element in this ternary alloy, is preferentially sputtered during bombardment. The resultant structure after bombarding is apparently a cubic CsCl type structure from analysis of the LEED pattern, which has two-fold symmetry, reflected through five axes (figure 19(*b*)). This was first observed by Zurkirch *et al* [76]. The STM image of this surface shows a rough, cluster-like surface (figure 19(*a*)) [77]. Quasicrystalline stoichiometry and order is restored by annealing the surface to higher temperatures, and the details of observations of these phases are discussed later.

4.2. Quasicrystalline phases

Annealing the surface to 725 K for 90 min produces a ten-fold symmetric LEED pattern. STM images taken after this preparation procedure show the surface to be terraced, but the terraces themselves are rough and characterized by random protrusions (figure 20(*a*)). The terraces have an average width of ∼100 Å. Annealing to 875 K improves the quality of the LEED patterns obtained (figure 20(*b*)) and the corresponding STM images show that the terraces are much larger (average width ∼450 Å) (figure 20(*c*)). The protrusions now appear to be three-fold symmetric and are preferentially orientated.

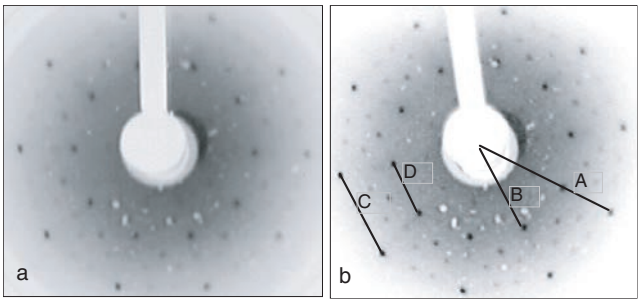

Figure 21. (*a*) LEED pattern obtained after annealing to 1125 K, taken at 79 eV, room temperature. (*b*) LEED pattern after annealing to 1125 K and sample cooled to 100 K. The peak positions are related by the golden number τ; A/B$=\tau$, C/D$=\tau$.

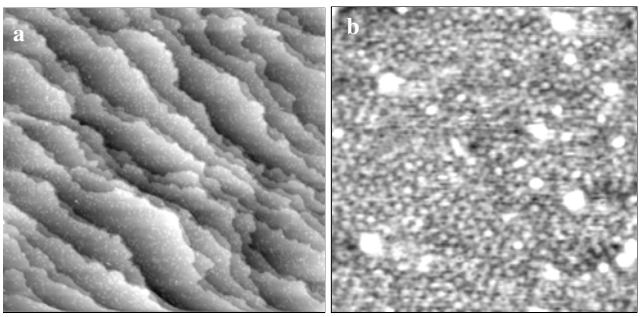

Figure 22. (*a*) 2000×2000 Å STM image after annealing to 1125 K—'flat' terraces. (*b*) 180×180 Å STM image after annealing to 1125 K.

As the annealing temperature increases so do the number, intensity and sharpness of the LEED spots, indicating increasing long-range order. The best quality LEED patterns have been obtained after the sample has been annealed to 1125 K—see figure 21. The patterns have ten-fold rotational symmetry with the peak positions being related by the golden number, τ, which is indicative of quasicrystallinity in the surface region. Since *d*-Al–Ni–Co is periodic perpendicular to the ten-fold direction, a single interlayer spacing is expected. Gierer *et al* [78] have deduced the interlayer spacing from their SPA-LEED data to be 2.04 Å. An average terrace width was also determined in that study to be 170 Å.

The STM images after this treatment indicate a surface which is much flatter—see figure 22. Atomically-resolved STM images show 2 nm decagonal clusters on the surface [79]. These results suggest that the surface has the same quasiperiodic structure as in the bulk—i.e. that the surface has a bulk-like termination, in agreement with x-ray photoelectron diffraction (XPD) and reflection high energy electron diffraction (RHEED) analyses [80]. Another recent STM study [81] has produced atomic resolution images of the surface after annealing the sample to 1175 K for 1–2 h. Those images show five-fold symmetric features which have opposite orientations in successive planes.

A correspondence can be drawn between the overlapping tiling model described in section 2.3 and the high-resolution STM images. Figure 23 shows an STM image decorated with overlapping decagons which have been chosen to coincide with the protrusions which form rings of 2 nm diameter. The decagons overlap in the ways shown in figure 5. It is possible to see evidence of the atomic structure inside the decagons.

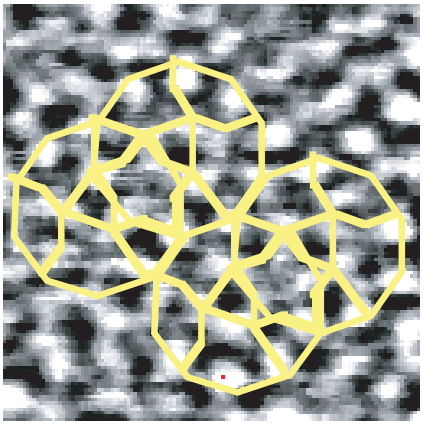

Figure 23. 50 Å × 50 Å STM image of the *d*-Al–Ni–Co showing a partial covering using the overlap rules described in [40].

4.3. Summary

Like the five-fold surface of *i*-Al–Pd–Mn, the ten-fold surface of *d*-Al–Ni–Co exhibits a crystalline phase after being sputtered, which progresses into a clustered surface structure upon annealing to relatively low temperatures, and finally forms a terraced phase at higher annealing temperatures ($\geqslant$725 K). The structure of the terraced phase observed in the STM images can be correlated with an overlapping decagonal tiling model.

5. Adsorption on quasicrystal surfaces

5.1. Introduction

The structural work described earlier indicates that the surfaces of quasicrystal materials may be prepared in a very perfect form with extended flat terraces and that they tend to confirm bulk structural models. One can therefore assert that the surfaces are fairly well understood. A natural progression from this is to see how the surface geometry is modified when adsorbates are present. This is potentially important from a technological perspective; for example it may be possible to improve frictional properties by forming a thin molecular coating of a suitable molecule (e.g. [82]). There is also the interesting possibility of whether a two-dimensional single species quasicrystalline overlayer can be formed. An atom or molecule adsorbing at a *unique* site on a quasicrystal surface could form such an overlayer by transference of the quasicrystallinity from the substrate 'template' to the adsorbate structure. Such overlayers would be very attractive for comparison with theoretical predictions of their expected symmetries [83], for the study of a wide range of electronic and dynamic phenomena in two dimensions (2D) [51], and as physical realizations of the inflation property of Penrose tilings [22]. To investigate these possibilities we chose model atomic and molecular adsorbates and studied their interaction with the *i*-Al–Pd–Mn surface.

5.2. Sulphur adsorption on i-Al–Pd–Mn

Although the question of how atomic adsorbates behave on a quasicrystal surface is an intriguing one, there has been little work on atomic adsorption geometry. If atomic adsorbates

formed ordered structures, reflecting the symmetry of the substrate, then the resulting overlayers would be fascinating examples of two-dimensional quasicrystalline systems. On the other hand, the multitude of possible adsorption sites present on a trimetallic aperiodic surface might lead to a disordered system. Sulphur is a good candidate atomic adsorbate for the formation of ordered overlayers, as it forms well-ordered structures on most metal and semiconductor surfaces.

The first work on sulphur adsorption on *i*-Al–Pd–Mn was reported by Ko *et al* [84]. In that study it was found that dosing at room temperature with sub-monolayer amounts of H_2S leads to the removal of the LEED pattern [84]. We have investigated sulphur adsorption on the five-fold surface of *i*-Al–Pd–Mn using AES, LEED, SPALEED and extended x-ray absorption fine structure (EXAFS) techniques. After dosing with sub-monolayer coverages of H_2S, we found that the LEED pattern disappears, in agreement with previous work [84]. Adsorption saturates at about monolayer coverage.

Near-edge EXAFS (NEXAFS) spectra (shown in figure 24) are very similar whether collected at a grazing or a normal incidence angle of the radiation [85]. As one expects a marked anisotropy in such spectra for S adsorbing in a single well-ordered adsorption site (see e.g. [86] for S adsorption on Ni(100)), this is an indication of either disordered adsorption or of adsorption at multiple sites, where the azimuthal polarization is averaged out. Surface EXAFS (SEXAFS) results from the same system show bonding both to surface Al and to subsurface Pd. Overall the results can be interpreted as indicating that multiple-site adsorption is taking place [85].

This is not such a surprising result, given the multitude of possible adsorption sites that must exist on such an aperiodic surface. This is especially true for an atomic adsorbate which is known to make strong chemisorption bonds. The best hope candidate for an atomic adsorbate which only occupies identical adsorption sites may be one which bonds weakly to the surface.

5.3. C_{60} adsorption on i-Al–Pd–Mn

To investigate molecular adsorption we chose C_{60} as a candidate adsorbate. C_{60} has been shown to improve the frictional properties of surfaces [82]. Additionally its cage diameter ($\sim$7 Å) is of the same magnitude as that of the pentagonal holes decorating the quasicrystalline surface used in these studies, which might lead to single-site adsorption under favourable preparation conditions. We have carried out extensive room temperature STM investigations of C_{60} adsorption on the five-fold surface of $Al_{70}Pd_{21}Mn_9$ combined with AES and SPALEED measurements [87].

At low coverages ($\sim$6.5% ML) a monodispersed phase is formed, with adsorption on the terraces and avoidance of step-edges. The preferred adsorption site is tentatively identified as the five-fold hollow. As the coverage is increased, a higher density layer is formed with no evidence of the formation of hexagonal ordered adsorbate structures as seen on several other substrates. This is followed by the onset of second layer formation.

We now focus on the low coverage surface (6.5% ML). Schaub and co-workers [52,64–66] have shown that the pentagonal hollows on the clean surface of the terraced phase are aligned along a Fibonacci pentagrid on the surface. This means that successive spacings of planes of these hollows have either long (L) or short (S) interplanar spacings, with the ratio of L to S being τ, the golden mean [28]. The distances between such hollows are subject to τ-scaling relationships: if the distance between two hollows on a line is multiplied by τ or powers of τ then the resulting distance locates other such hollows along the same line. The minimum distance between the centres of such hollows is 11 ± 2 Å. Several examples (chosen to elucidate the C_{60} results described later) are shown in figure 25(*a*); the distances

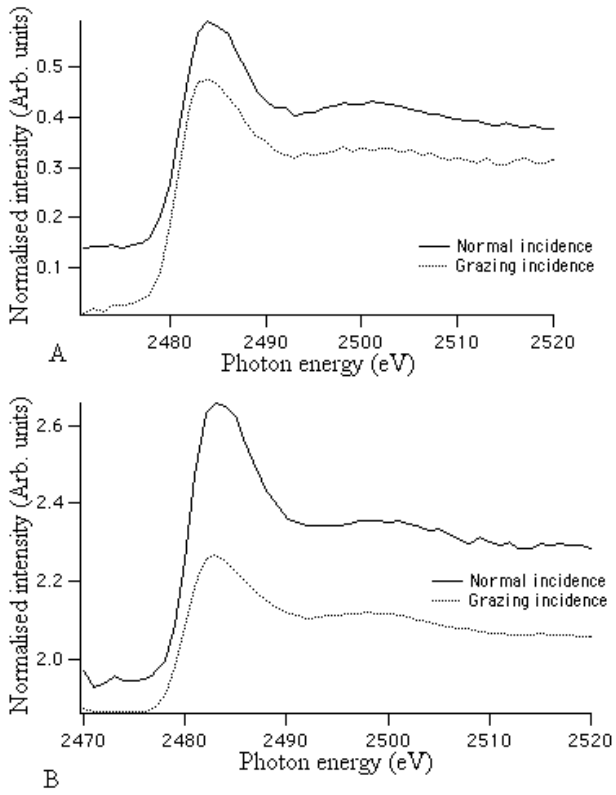

Figure 24. S K-edge NEXAFS at normal and grazing incidence for *i*-Al–Pd–Mn surfaces annealed for 150 min to (*a*) 790 K (clustered phase of section 3.2.4) and (*b*) 970 K (terraced phase of section 3.2.5); from [85].

[AB] = 30 ± 5 Å, [AC] = 50 ± 5 Å, [AD] = 85 ± 5 Å and [AE] = 141 ± 5 Å. Thus within experimental error

$$[\mathrm{AE}] = \tau[\mathrm{AD}] = \tau^2[\mathrm{AC}] = \tau^3[\mathrm{AB}] \tag{3}$$

and similarly:

$$[\mathrm{EH}] = \tau[\mathrm{EG}] = \tau^3[\mathrm{EF}]. \tag{4}$$

Although the clean surface areas are not resolved as well in figure 25(*a*), (due to the presence of the C_{60} molecules), it is possible to locate the five-fold pentagonal hollows because of their size. It can be seen that the C_{60} molecules are aligned along the same directions as the pentagonal hollows. The figure is labelled such that the visible hollows labelled A′, B′ and D′, and the distances between them, are exactly as for A, B and D on the clean surface in figure 25(*a*); now it can be seen that C_{60} molecules are adsorbed in the positions C′, E′, F′, G′ and H′, i.e. directly on-top of the underlying pentagonal hollows. This means that the τ-scaling relationships found in figure 25(*a*) are transferred to the C_{60} molecules; for example equation (4) applies now to the C_{60} molecules in the form:

$$[\mathrm{E'H'}] = \tau[\mathrm{E'G'}] = \tau^3[\mathrm{E'F'}]. \tag{5}$$

Therefore we can conclude that at low coverages, pentagonal hollows are identified as preferential adsorption sites for C_{60} adsorption. However at higher coverages it was not

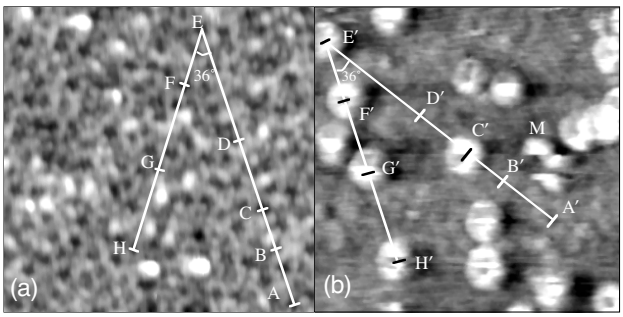

Figure 25. (*a*) 150 × 150 Å STM image of the flat $Al_{70}Pd_{21}Mn_9$ surface (1.97 V, 1.04 nA). Sequences of pentagonal hollows labelled A, B, . . . , H along two directions are indicated. The angle between these two lines is present in a Fibonacci pentagrid. (*b*) 150 × 150 Å STM image of the flat $Al_{70}Pd_{21}Mn_9$ surface at a coverage of 6.5% (1.97 V, 1.04 nA). C_{60} molecules adsorb on the pentagonal hollows, leading to τ-scaling relationships between the molecules; after [87].

possible to form a two-dimensional quasicrystalline overlayer; either the density of molecules was too small to observe the expected correlations at low coverages, or multiple sites are occupied at higher coverages. The relatively large cage diameter of C_{60} molecules in any case leads to site blocking at the lower coverages which mitigates against the formation of a denser overlayer with occupation of the favourable five-fold sites.

5.4. Summary

From the results discussed earlier (and other studies not described) it is possible to surmise that the best candidate adsorbates for the formation of ordered overlayer systems (among the atomic and molecular species tried so far) are those which do not have a strong chemisorption interaction with the quasicrystalline substrate. When such a strong interaction does take place, it appears that the quasicrystalline structure of the surface is inevitably destroyed. It should be noted that there is another class of adsorbates, i.e. those which are metallic, which show promising signs of pseudomorphic growth. Shimoda *et al* have shown that surfactant-mediated Au growth on the quasicrystalline *i*-Al–Pd–Mn surface results in a Au–Al alloy film which has quasicrystalline order [88].

6. Concluding remarks

The discovery of quasicrystals has led to a major and very active research field in condensed matter physics, with a number of International Conference Series devoted to the topic which attract hundreds of participants (e.g. the International Conference on Quasicrystals and the International Conference on Aperiodic Crystals). The number of attendees at these meetings interested in the surfaces of quasicrystals has grown considerably in the past few years, thanks in part to the development of the ability to grow samples large enough for analysis using conventional surface science tools. In this paper we have given a brief (and by no means comprehensive) overview of some topics of current interest in this area. It appears that a good understanding has been attained of clean surface structure, at least in the cases of *i*-Al–Pd–Mn and *d*-Al–Ni–Co. Attention is now turning to the characterization of adsorption systems and the possible uses of these surfaces, perhaps even as templates for a ‘quasicrystal nanotechnology’.

Acknowledgments

We thank Professor Pat Thiel, Dr Cynthia Jenks, Dr Tom Lograsso, Dr Amy Ross, N Kelso and Dr Paul Canfield of the quasicrystals program at the Ames Laboratory, Iowa, for continued support. We acknowledge Dr Zorka Papadopolos and Dr Gerald Kasner of the University of Magdeburg for many stimulating discussions. The EPSRC (grant numbers GR/N18680), NSF (grant number DMR-9819977) are acknowledged for funding. The EPSRC supports a Physics Network on Quasicrystal Surfaces (GR/N25718, 2000-2003) which is coordinated from the University of Liverpool. Further information on this Network is available at http://svr.ssci.liv.ac.uk/ quasi/.

References

[1] Ashcroft N W and Mermin N D 1976 *Solid State Physics* (Fort Worth: Saunders)
[2] Shechtman D, Blech I, Gratias D and Cahn J W 1984 *Phys. Rev. Lett.* **53** 1951
[3] Shechtman D and Lang C I 1997 *Mater. Res. Soc. Bull.* **22** 40
[4] Pauling L 1985 *Nature* **317** 512
[5] 1992 *International Union of Crystallography, Acta Crystallographia* A **48** 922
[6] Tsai A P, Guo J Q, Abe E, Takakura H and Sato T J 2000 *Nature* **408** 537
[7] Rotenberg E, Theis W, Horn K and Gille P 2000 *Nature* **406** 602
[8] Tsai A P and Yoshimura M 2001 *Mater. Res. Soc. Symp. Proc.* **643** K16.4
[9] Dubois J M 1993 *Phys. Scr.* T **49A** 17
[10] von Stebut J, Soro J M, Plaindoux P and Dubois J M 1997 *New Horizons in Quasicrystals: Research and Applications* ed A I Goldman, D J Sordelet, P A Thiel and J M Dubois (Singapore: World Scientific) p 248
[11] Dubois J M, Plaindoux P, Belin-Ferré E, Tamura N and Sordelet D J 1998 *Proc. 6th. Int. Conf. on Quasicrystals* ed S Takeuchi and T Fujiwara (Singapore: World Scientific) p 451
[12] Rivier N and Boose D 1995 *Proc. 5th. Int. Conf. on Quasicrystals* ed C Janot and R Mosseri (Singapore: World Scientific) p 802
[13] Gibbons P C and Kelton K F 1999 Physical properties of quasicrystals *(Springer Series in Solid State Sciences)* ed Z M Stadnick (Berlin: Springer) pp 403–31
[14] Gahler F, Kramer P, Trebin H-R and Urban K (ed) 2000 *Proc. 7th Int. Conf. on Quasicrystals (Guest Mat. Sci. Eng.)* A pp 294–6
[15] Moriarty P 2001 *Rep. Prog. Phys.* **64** 297
[16] Parker G and Charlton M 2000 *Phys. World* **13** 29
[17] Grünbaum B and Shephard G C 1987 *Tilings and Patterns* (San Francisco: Freeman)
[18] Crowe D W 1992 *Fivefold Symmetry* ed I Hargittai (Singapore: World Scientific) p 465
[19] Makovicky E 1992 *Fivefold Symmetry* ed I Hargittai (Singapore: World Scientific) p 67
[20] Kepler J 1619 *Harmonices Mundi* (Joannes Plancus, Lincii Austria)
[21] Casper D L D and Fontano E 1996 *Proc. Natl Acad. Sci. USA* **93** 14 271
[22] Penrose R 1974 *Bull. Inst. Math. Appl.* **10** 266
[23] Penrose R 1989 *The Emperor's New Mind—Concerning Computers, Minds, and The Laws of Physics* (Oxford: Oxford University Press) p 136
[24] Durand E 2001 *Preprint* http://www.geom.umn.edu/apps/quasitiler/
[25] Kramer P, Papadopolos Z and Teuscher H 1999 *J. Phys.: Condens. Matter* **11** 2729
[26] Senechal M 1995 *Quasicrystals and Geometry* (Cambridge: Cambridge University Press)
[27] Janot C 1998 *Quasicrystals, A Primer* 2nd edn (Oxford: Clarendon)
[28] See e.g. Dunlop R A 1997 *The Golden Ratio and Fibonacci Numbers* (Singapore: World Scientific)
[29] Katz A and Gratias D 1995 *Proc. 5th Int. Conf. on Quasicrystals* ed C Janot and R Mosseri (Singapore: World Scientific) pp 164–7
[30] Elser V 1996 *Phil. Mag.* B **73** 641
[31] Papadopolos Z, Kramer P and Liebermeister W 1998 *Proc. Int. Conf. on Aperiodic Crystals, Aperiodic 1997* ed M de Boissieu, J-L Verger-Gaugry and R Currant (Singapore: World Scientific) pp 173–81
[32] Kasner G, Papadopolos Z, Kramer P and Bürgler D E 1999 *Phys. Rev.* B **60** 3899
[33] Papadopolos Z, Kramer P, Kasner G and Bürgler D E 1999 *Mater. Res. Soc. Symp. Proc.* **553** 231
[34] Quiquandon M, Calvayrac Y, Quivy A, Faudot F and Gratias D 1999 *Mater. Res. Soc. Symp. Proc.* **553** 95

[35] Boudard M and de Boissieu M 1999 *Physical Properties of Quasicrystals* ed Z M Stadnik (New York: Springer) pp 119–24
[36] Steinhardt P J, Jeong H-C, Saitoh K, Tanaka M, Abe E and Tsai A P 1998 *Nature* **396** 55
[37] Burkov S E 1991 *Phys. Rev. Lett.* **67** 614
[38] Jeong H-C and Steinhardt P J 1997 *Phys. Rev.* B **55** 3520
[39] Gummelt P 1996 *Geom. Dedicata* **62** 433
[40] Abe E, Takakura H, Tsai A P, Steinhardt P J and Jeong H-C 2000 *Phys. Rev. Lett.* **84** 4609
[41] Hiraga K, Ohsuna T and Nishimura S 2001 *Phil. Mag. Lett.* **81** 123
[42] Hiraga K, Ohsuna T, Nishimura S and Kawasaki M 2001 *Phil. Mag. Lett.* **81** 109
[43] Tsuda K, Nishida Y, Saitoh K and Tanaka M 1996 *Phil. Mag.* A **74** 697
[44] Saitoh K, Tsuda K and Tanaka M 1999 *Mater. Res. Soc. Symp. Proc.* **553** 177
[45] Ebert Ph, Feuerbacher M, Tamura N, Wollgarten M and Urban K 1996 *Phys. Rev. Lett.* **18** 3827
[46] Ebert Ph, Yue F and Urban K 1998 *Phys. Rev.* B **57** 2821
[47] Ebert P, Kluge F, Grushko B and Urban K 1999 *Phys. Rev.* B **60** 874
[48] Delaney D W, Bloomer T E and Lograsso T A 1997 *New Horizons in Quasicrystals: Research and Applications* ed A I Goldman, D J Sordelet, P A Thiel and J M Dubois (Singapore: World Scientific) p 45
[49] Ledieu J, McGrath R, Diehl R D, Lograsso T A, Delaney D, Papadopolos Z and Kasner G 2001 *Surf. Sci. Lett.* **492/493** L729
[50] Jenks C J, Burnett J W, Delaney D W, Lograsso T A and Thiel P A 2000 *Appl. Surf. Sci.* **157** 23
[51] Zangwill A 1988 *Physics at Surfaces* (Cambridge: Cambridge University Press)
[52] Schaub T M, Bürgler D E, Güntherodt H-J and Suck J-B 1994 *Z. Phys.* B **96** 93
[53] Bolliger B, Erbudak M, Vvedensky D D, Zurkirch M and Kortan A R 1998 *Phys. Rev. Lett.* **80** 5369
[54] Bolliger B, Erbudak M, Hensch A, Kortan A R and Vvedensky D D 1999 *Mater. Res. Soc. Symp. Proc.* **553** 257
[55] Shen Z, Kramer M J, Jenks C J, Goldman A I, Lograsso T, Delaney D, Heinzig M, Raberg W and Thiel P A 1998 *Phys. Rev.* B **58** 9961
[56] Jenks C J 1999 *Mater. Res. Soc. Symp. Proc.* **553** 219
[57] Ledieu J, Munz A W, Parker T M, McGrath R, Diehl R D, Delaney D W and Lograsso T A 1999 *Surf. Sci.* **433/435** 665
[58] Ledieu J 2001 *PhD Thesis* The University of Liverpool
[59] Shen Z, Stoldt C R, Jenks C J, Lograsso T A and Thiel P A 1999 *Phys. Rev.* B **60** 14 688
[60] Zurkirch M, Bolliger B, Erbudak M and Kortan A R 1998 *Phys. Rev.* B **58** 14 113
[61] Guyot P, Kramer P and de Boissieu M 1991 *Rep. Prog. Phys.* **54** 1373
[62] Ledieu J, Munz A W, Parker T M, McGrath R, Diehl R D, Delaney D W and Lograsso T A 1999 *Mater. Res. Soc. Symp. Proc.* **553** 237
[63] Jenks C, Delaney D W, Bloomer T E, Chang S-L, Lograsso T A, Shen Z, Zhang C-M and Thiel P A 1996 *Appl. Surf. Sci.* **103** 485
[64] Schaub T M, Bürgler D E, Güntherodt H-J and Suck J-B 1994 *Phys. Rev. Lett.* **73** 1255
[65] Schaub T M, Bürgler D E, Güntherodt H-J, Suck J B and Audier M 1995 *Appl. Phys.* A **61** 491
[66] Schaub T M, Bürgler D E, Schmidt C M and Güntherodt H-J 1996 *J. Non-Cryst. Solids* **205/207** 748
[67] Gierer M, Van Hove M A, Goldman A I, Shen Z, Chang S-L, Pinhero P J, Jenks C J, Anderegg J W, Zhang C-M and Thiel P A 1998 *Phys. Rev.* B **57** 7628
[68] Gierer M and Over H 1999 *Z. Kristallogr.* **214** 14
[69] Boudard M, de Boissieu M, Janot C, Heger G, Beeli C, Nissen H-U, Vincent H, Ibberson R, Audier M and Dubois J M 1992 *J. Phys.: Condens. Matter* **4** 10 149
[70] Gierer M, Van Hove M A, Goldman A I, Chang S-L, Shen W Z, Zhang C-M, Jenks C J and Thiel P A 1997 *Phys. Rev. Lett.* **78** 467
[71] Ledieu J, Muryn C A, Thornton G, Cappello G, Chevrier J, Diehl R D, Lograsso T A, Delaney D and McGrath R 2000 *Mater. Sci. Eng.* A **294–6** 871
[72] Taylor M A 1961 *Acta Crystallogr.* **14** 84
[73] Bolliger B, Erbudak M, Vvedensky D D and Kortan A R 1999 *Phys. Rev. Lett.* **82** 763
[74] Cappello G *et al* 1999 *Mater. Res. Soc. Symp. Proc.* **553** 243
[75] Naumović D, Aebi P, Schlapbach L and Beeli C 1997 *New Horizons in Quasicrystals: Research and Applications* ed A I Goldman, D J Sordelet, P A Thiel and J M Dubois (Singapore: World Scientific)
[76] Zurkirch M, Bolliger B and Erdubak M 1998 *Phys. Rev.* B **58** 14 113
[77] Cox E J, Ledieu J, McGrath R, Diehl R D, Jenks C J and Fisher I 2001 *Mater. Res. Soc. Symp. Proc.* **643** K11.3
[78] Gierer M, Mikkelsen A, Gräber M, Gille P and Moritz W 2000 *Surf. Sci.* **463** L654
[79] Cox E J, Ledieu J, McGrath R, Diehl R D, Jenks C J, Kelso N and Canfield P 2002 in preparation
[80] Shimoda M, Guo J Q, Sato T J and Tsai A-P 2000 *Surf. Sci.* **454–6** 11

[81] Kishida M, Kamimura Y, Tamura R, Edagawa K, Takeuchi S, Sato T, Yokoyama Y, Guo J Q and Tsai A P 2002 submitted
[82] Allers W, Hahn C, Lohndorf M, Lukas S, Pan S, Schwarz U D and Wiesendanger R 1996 *Nanotechnology* **7** 346
[83] Lifshitz R 1996 *Physica* A **232** 633
[84] Ko J S, Gellman A J, Lograsso T A, Jenks C J and Thiel P A 1999 *Surf. Sci.* **423** 243
[85] Ledieu J, McGrath R, Dhanak V R, Diehl R D, Lograsso T A and Delaney D W 2002 submitted
[86] McGrath R, MacDowell A A, Hashizume T, Sette F and Citrin P H 1989 *Phys. Rev.* B **40** 9457
[87] Ledieu J, Muryn C A, Thornton G, Diehl R D, Lograsso T A, Delaney D W and McGrath R 2001 *Surf. Sci.* **472** 89
[88] Shimoda M, Guo J Q, Sato T J and Tsai A P 2001 *Mater. Res. Soc. Symp. Proc.* **643** K11.5